Chapter 3

Speeding up biomolecular interactions by molecular sledding

Numerous biological processes involve association of a protein with its binding partner, an event that is preceded by a diffusion-mediated search bringing the two partners together. Often hindered by crowding in biologically relevant environments, three-dimensional diffusion can be slow and result in long bimolecular association times. Similarly, the initial association step between two binding partners often represents a rate-limiting step in biotechnologically relevant reactions. We demonstrate the practical use of an 11-a.a. DNA-interacting peptide derived from adenovirus to reduce the dimensionality of diffusional search processes and speed up associations between biological macromolecules. We functionalise binding partners with the peptide and demonstrate that the ability of the peptide to one-dimensionally diffuse along DNA results in a 20-fold reduction in reaction time. We also show that modifying PCR primers with the peptide sled enables significant acceleration of standard PCR reactions

Alexander Turkin, Lei Zhang, Alessio Marcozzi, Walter F. Mangel, Andreas Herrmann, Antoine M. van Oijen

Published in: *Chemical Science* DOI: 10.1039/C5SC03063C (2015).

3.1. Introduction

The crowded intracellular environment presents many challenges for basic molecular processes to occur. Non-specific interactions between proteins hinder diffusional mobility and increase the time needed for binding partners to find each other and associate.[1] Nature displays several examples in which the dimensionality of search processes is reduced to speed up association times.[2] For example, binding partners of certain classes of cell-surface receptors associate with lipid membranes and utilise two-dimensional diffusion to promote association.[3] Many DNA-interacting proteins find specific sequences or lesions in large amounts of nonspecific DNA by performing one-dimensional random walks along the DNA.[4] Every time such a protein associates with DNA, it transiently diffuses along the duplex and thus drastically increases the number of sampled DNA positions per unit of time. It then dissociates from the DNA, undergoes three-dimensional (3D) diffusion through solution to rebind at an entirely different region and again searches a stretch by one-dimensional (1D) diffusion. The combination of 3D and 1D searches gives rise to a drastic increase in the effective bimolecular association rate constant of the protein with its target.[5,6]

An example of a naturally occurring system in which 1D diffusion along DNA is used to speed up association between two proteins is found in adenovirus.[7,8] During viral maturation, a large number of proteins within a single viral particle need to be proteolytically processed by the adenovirus protease (AVP) before infection of a cell.[9] Tight packing of protein and DNA within the viral particle makes regular 3D diffusion as a mechanism for the protease to travel from one target to the other impossible. Recent work has shown that the AVP protein[10] recruits the short 11-a.a. pVIc peptide (GVQSLKRRRCF),[11] itself a proteolytic product in early maturation, and uses it to slide along the DNA inside the viral particle and thus effectively reduces the search space for the protease from three dimensions to one.[8]

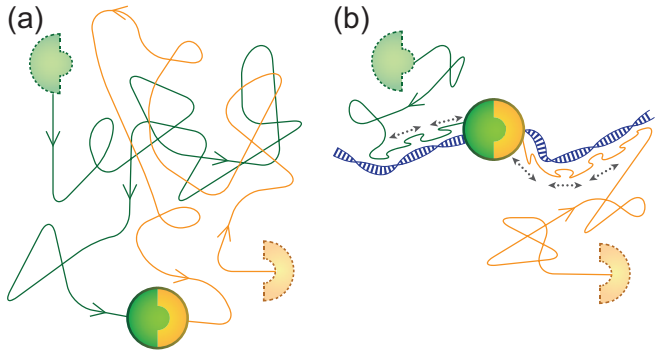

Figure 3.1 | Speeding up association between biomolecules using the ability of a 'sled' peptide to one-dimensionally diffuse along DNA. (a) Usually, association between molecules occurs as a result of binding partners finding each other by diffusion in a 3D fashion through solution. (b) Addition of a 1D reaction pathway can drastically speed up the reaction by reducing the dimensionality of search.

3.2. Results and discussion

In this work we demonstrate that the ability of the pVIc peptide to slide along DNA can be used to speed up a much broader class of biomolecular processes than just those occurring *in vivo* and that it can be used to dramatically improve the speed of common laboratory reactions (Fig. 3.1). First, as a proof of principle, we couple each of the two binding partners in a canonical biotin-streptavidin association to the pVIc 'molecular sled' and show that association proceeds more than an order of magnitude faster in the presence of DNA (Fig. 3.2a). Fluorescence Resonance Energy Transfer (FRET)[12] was used to monitor the time dependence of the bimolecular association. For simplicity, we refer to the functionalised biotin and streptavidin as binding partners *B* and *S*, respectively. Binding partner *B* is formed by reacting a maleimide-functionalised biotin with the cysteine Cys10' of Cy3-labelled pVIc in a Michael-addition reaction (see section 3.4, Fig. 3.5). The maleimide and biotin units are connected via a high-molecular weight polyethylene glycol (PEG) linker resulting in a total molecular weight for binding partner *B* of 6.7 kDa. This high molecular weight reduces its

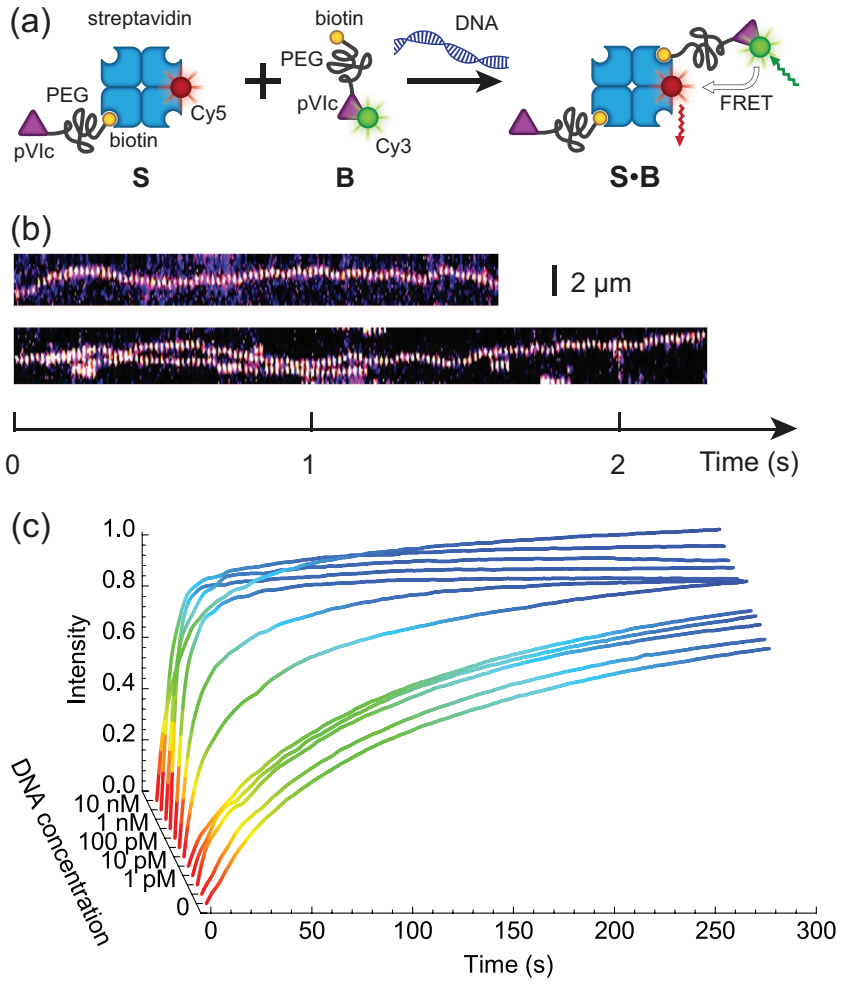

Figure 3.2 | Speeding up bimolecular association by DNA. (a) A schematic of the proof-of-concept biotin-streptavidin system. (b) Single-molecule fluorescence imaging confirms that functionalisation of binding partners with pVIc peptide renders *S* and *B* able to 1D slide along DNA. The results are presented as kymographs: top trace shows the sliding of binding partner *S*, bottom trace shows the sliding of binding partner *B*, labelled with streptavidin-Cy5 for the ease of detection in view of the signal-to-noise ratio. (c) The formation of complex *S•B* is monitored in time using various concentrations of 2686-bp long DNA in solution. The time evolution of product concentration can be approximated by exponential growth $C(t) = C_{\max}\left[1 - \exp(-t/\tau)\right]$, where τ is the observed characteristic reaction time.

diffusional mobility and allows us to more easily gain access to the timescale of association. Binding partner *S* is prepared by forming a complex between a Cy5-labelled tetrameric streptavidin and an unlabelled biotin-pVIc conjugate (see section 3.4). The ability of both *B* and *S* to 1D diffuse along DNA was confirmed on a single-molecule level using Total Internal Reflection Fluorescence (TIRF) microscopy (Fig. 3.2b, see section 3.4 for experimental conditions and notes). We estimated the binding times $\tau_{1D} \approx 0.3\,\mathrm{s}$ and the 1D diffusion coefficient $D_{1D} \approx 3\times10^{4}\,\mathrm{nm^2/s}$. Using these values, we can calculate that *S* and *B* are able to explore a DNA segment of length $L_{1D} = \sqrt{2D_{1D}\tau_{1D}} \approx 130\,\mathrm{nm} \approx 400\,\mathrm{bp}$ before dissociating and returning to solution.

Binding partners *B* and *S* were combined in aqueous solution at final concentrations of 150 nM and 37.5 nM, respectively, and ensemble FRET between the Cy3 donor and Cy5 acceptor fluorophores was measured (Fig. 3.6). Fig. 3.2c shows the time dependencies of bimolecular association in the presence of 2686-bp long double-stranded DNA (dsDNA) at different concentrations. Addition of the DNA up to 1 pM did not have a significant effect on the reaction rate, whereas DNA concentrations of higher than 10 pM resulted in a clearly discernable reduction of the reaction time. For a DNA concentration of 300 pM, already after 15 s 99% of the maximum FRET efficiency was achieved.

Fig. 3.3a shows the reaction times as derived from the FRET traces for different DNA concentrations and lengths. For each length, varying from 2,686 to 15 base pairs (Table 3.1), the association times decrease by up to 20-fold at higher concentrations of added DNA. Interestingly, the critical concentration for reaction speed up differs for the different DNA lengths: longer DNA fragments are required at lower concentrations than short DNA molecules to achieve the same catalytic effect. This behaviour can be explained by the fact that the critical number of reaction partners associated with DNA is reached at higher DNA concentrations for short fragments and at low DNA concentrations for longer pieces of DNA. Thus, the main parameter that governs the kinetics of reaction is the total base pair concentration, a unit that describes the total length of DNA per

unit volume. This notion is validated by plotting the reaction time against DNA base pair concentration (Fig. 3.3b), showing the curves cluster together in three distinct regions. These regimes can be understood in terms of the density of binding partners trapped on the catalytic DNA molecules. At low base pair concentrations, the amount of DNA available per binding partner is too low to trap a noticeable fraction of the binding partners and influence the overall reaction rate. In the optimal regime, around 0.1 to 10 μM of base pairs, the binding partners have high probability to be trapped by DNA where they can find each other by 1D diffusion. At base pair concentrations higher than 100 μM, the probability for binding partners *B* and *S* to bind to the same DNA molecule diminishes, resulting in a deceleration of the association.

In an alternative mechanism to explain the increased association rates, DNA-bound binding partners bound to the same DNA molecule could be brought into proximity of each other by bending and looping of the DNA duplex. In such a mechanism, the binding partners would rely on the conformational flexibility of the DNA and use the duplex as a scaffold to bring binding partners together. In order to exclude this pathway, we conducted a series of experiments with DNA of four different lengths (50, 100, 150 and 300 bp), which were chosen such that the corresponding DNA looping probability differed significantly from one another.[13,14] Under the low-salt buffer conditions used in this study, DNA molecules of 50 and 100 bp can be regarded as stiff rods whose folding onto itself is excluded (DNA persistence length is estimated to be 250 bp at 2 mM NaCl).[15] In case looping was the main mechanism for reaction speed-up one would expect a considerably lower reaction acceleration in case of 50 and 100 bp long DNA as compared to 300 bp, which is long enough to form loops. However, in all cases we observed the same 20-fold reaction speed-up (Fig. 3.3a and 3.3b), confirming that association is not mediated by DNA bending onto itself.

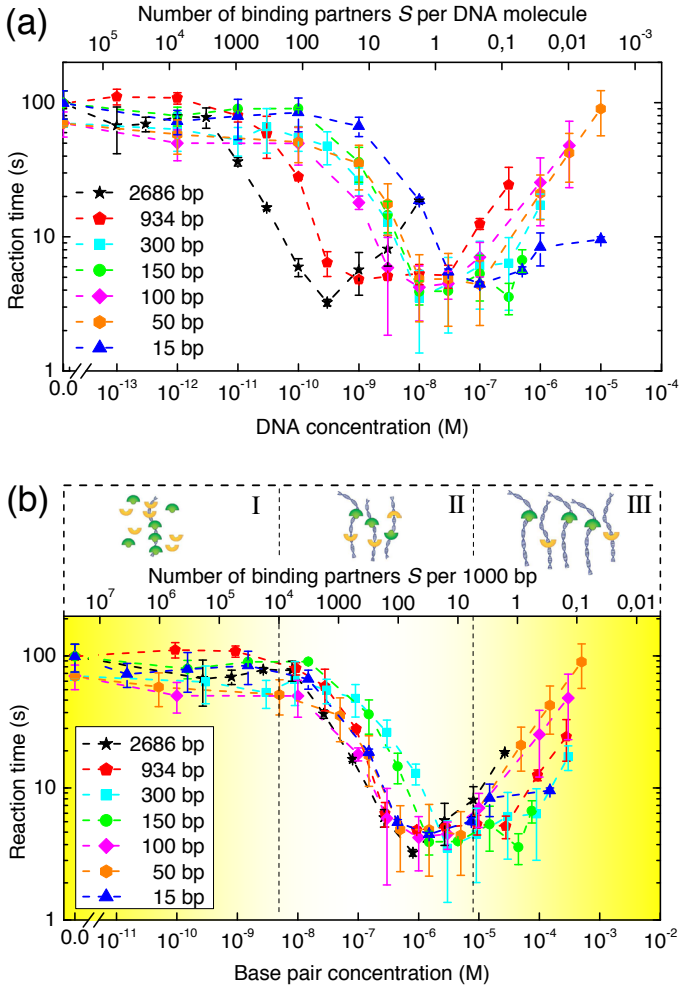

Figure 3.3 | Influence of DNA length and concentration on the reaction time. (a) Biotin-streptavidin association experiments are repeated for different DNA lengths. Reaction times τ are presented as a function of DNA concentration. (b) Plotting the dependencies of the reaction times on DNA base pair concentration results in curve clustering together in three regions: I) no speed-up due to an insufficient number of DNA molecules per binding partner; II) maximum speed-up with the optimal amount of DNA per binding partner; III) reduced speed-up caused by the amount of DNA being so high that the probability of binding partners to meet on the same DNA molecule diminishes. Error bars indicate ±SD; $n \geq 3$.

Using a similar reasoning, one could argue that the conformational flexibility of the long PEG linkers attached to both binding partners allows those binding partners that are statically but distally bound to the same DNA to associate without the need for sliding. Fig. 3.3b shows, however, a 10-fold increase in reaction time at a reaction stoichiometry as low as 1 binding partner per 1,000 base pairs, clearly an average molecular separation too high to be bridged by the binding partners statically bound to the same DNA. From the considerations above, one can conclude that sliding along DNA, and not just static binding, is responsible for the increase in association rate.

An understanding of the origin of the reaction acceleration effect can be obtained from our recent work in which we formulated a kinetic model for a system with linear sinks (i.e. DNA) that can intermittently trap molecules present in a solution and serve as an assembly line for 1D diffusing molecules.[16] Our model semiquantitatively predicts the experimentally observed speed-up in the presence of DNA molecules of different lengths and concentrations. Moreover, according to our simulations, the relative contribution of the 1D reaction pathway in the optimum speed-up regime can be as high as 90%. In this work, we concluded that although association of the binding partners on DNA without 1D sliding does play a role, the primary contributor to the reaction acceleration is a 1D sliding mechanism. This model also shows that in the case of extremely short DNA molecules (15 bp and 50 bp), the reaction acceleration cannot be explained by 1D sliding alone due to the sizes of the binding partners being comparable to the dimensions of the DNA. Instead, reaction acceleration is introduced by the high diffusional mobility of the short DNA duplexes and their ability to electrostatically capture the cationic peptides.[16]

As a next step, we set out to use our method to speed up a standard polymerase chain reaction (PCR) by reducing the time needed for pVIc-coupled primers to anneal to the template DNA. The exponential amplification of DNA during PCR can be divided into three distinct steps.[17] The first step is the melting of the double-stranded DNA template (Fig. 3.4a), followed by primer annealing and elongation with the polymerase. During the annealing step, primers need to

find and hybridise to their complementary target sequence on a template. During this annealing step, the DNA will consist of a mixture of denatured and double-stranded regions, providing a large variety of structures for the pVIc-primers to interact with and potentially move along, resulting in a reduction of the time needed for the primer to locate and bind to its target sequence.

We covalently coupled (see section 3.4) the pVIc peptide to the 5' ends of a pair of PCR primers (primer set I, Table 3.2, Fig. 3.7 and 3.8) designed to amplify a 807-bp stretch from a linear double-stranded 1970-bp-long template and used real-time PCR (qPCR) experiments with SYBR Green I fluorescence to report on the kinetics of amplicon formation[18] (Fig. 3.4b and 3.9). The correct length of the PCR product was confirmed by agarose gel electrophoresis (Fig. 3.10). Similar results were obtained for PCR experiments employing a different pair of primers (Table 3.2, Fig. 3.11) and a longer 8669-bp-long circular template M13KO7 (Fig. 3.12). The kinetics of amplicon formation were quantified in an unbiased manner by employing a PCR threshold cycle analysis (see section 3.4, Fig. 3.13). Remarkably, the PCR reaction containing the pVIc-conjugated primers displayed a significant reduction in the number of cycles needed, suggesting the use of a molecular sled as a viable approach to speed up the overall reaction time of PCR. In our experiments we were able to shorten the PCR reaction time by 15%~27%. To ensure that the increase in speed is not caused by a nonspecific electrostatic association between the four positively charged amino acids in the sliding peptide and the negatively charged DNA backbone, we repeated the same PCR experiments using primers conjugated to a scrambled peptide (S-peptide, SFRRCGLRQVK) containing the same residues in a random order, which presumably affects the sliding behaviour of the peptide yet preserving the net charge. Our qPCR data reveals that use of primers conjugated with this scrambled peptide does not result in a decrease of the number of PCR cycles required for amplification (Fig. 3.4b, 'S-peptide').

The performance of the S-peptide-modified primers is very similar to the unmodified primers. Furthermore, we observed a significant reduction in the number of PCR cycles when using a truncated pVIc variant containing only the

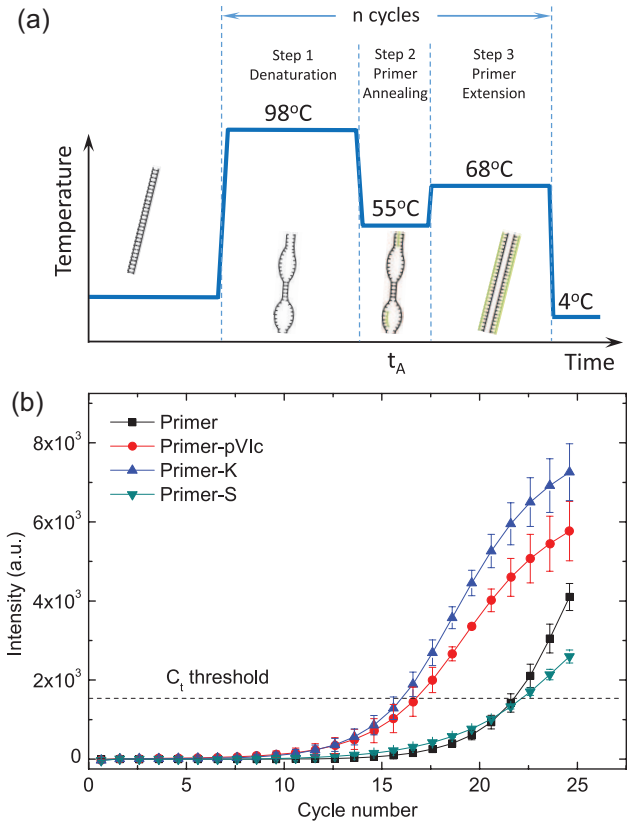

Figure 3.4 | Speed-up of PCR by sled-modified primers. During the annealing step of a thermal cycling PCR protocol (a), primers need to find and hybridise to their complement on a template. This process can be accelerated by attaching the pVIc sled peptide to PCR primers. (b) Amplicon formation for different primer-peptide conjugates is shown for annealing time t_A = 1s and primer concentration C_{primer} = 0.125 µM. The C_t threshold values for PCR reactions using unmodified primers, primer-S (negative control), primer-pVIc and primer-K were measured to be 21.7 ± 0.4, 22.1 ± 0.2, 16.7 ± 0.7, and 16 ± 0.5, respectively. Error bars indicate ±SD; n = 3.

last six amino acids of pVIc, four of which are positively charged and are sufficient to support sliding along DNA (Fig. 3.4b, K-peptide, KRRRCF, Fig. 3.14). Finally, we studied the behaviour of the primer modifications under different conditions by varying the annealing time t_A and primer concentration C_{primer} (Fig. 3.12). In

case of the most stringent conditions (short annealing time, low primer concentration) the effect of the sliding peptides was the most pronounced.

To exclude a scenario in which the acceleration effect could originate from the enhanced primer-template binding due to cationic nature of the peptides, we compared the melting temperatures T_m of the modified and unmodified primers that were used in the PCR experiments. When using short complementary oligonucleotides, and thus excluding sliding contributing to affinity, the measured T_m values of the peptide-functionalised primers were identical to those of the non-functionalised ones (Fig. 3.15). This observation excludes an enhanced stability of binding to DNA in the PCR reactions because of the peptide.

The use of chimeric molecules, where the desired functions of parent moieties are combined within one molecule is a well-established approach in biotechnology. In PCR, for example, attempts have been made to increase the affinity of primers and polymerases to DNA by functionalising primers with DNA-intercalating molecules[19,20] and expressing the polymerases with an additional cationic peptide motif in the sequence.[21-24]

The enhancement of molecular activity in these cases arises from the increase of the attractive electrostatic and intermolecular forces between the desired molecule and DNA. Another approach that uses the same concept of chimeric molecules is DNA-templated synthesis, where the binding partners are conjugated to single-stranded DNA oligonucleotides and are physically brought into proximity of one another by hybridising them to a DNA template.[25-27] In our study, however, the mechanism of activity enhancement is different from these approaches: as opposed to increasing the affinity between the binding partners by prolonging the dissociation time, we aimed to speed up association by addition of a different reaction pathway – 1D diffusion along DNA. The reduction of search dimensionality makes the binding partners find each other faster and, thus, results in the overall reaction acceleration.

3.3. Conclusions

Summarising, the 11-a.a. DNA-interacting pVIc peptide acts as a molecular sled in speeding up biochemical reactions by introducing a 1D reaction pathway in addition to bimolecular association via 3D diffusion. Our demonstration of the speed up of both a highly generalised reaction and a commonly used laboratory process suggests a wide variety of other potential uses.

3.4. Experimental section

3.4.1. Preparation of the binding partners

Stock solution of binding partner *B* was prepared as follows. N-terminus Cy3 labelled pVIc (custom peptide synthesis by Bio-Synthesis, Inc), 50 μM, was derivatised at Cys10' in 25 mM PBS buffer (pH 7.3) by adding biotin-PEG-maleimide (5 kDa, Nanocs) to 50 μM. The reaction vial was wrapped in aluminium foil to protect from light and the reaction was allowed to proceed for 5 hours at room temperature on a nutator. The reagent was subsequently stored at $+4^0$C and used as is without further purification over the course of one month. Successful conjugation was confirmed by MALDI/TOF mass spectrometry (Fig. 3.5).

3.4.2. Spectrofluorometer assay

The experiments were performed in the sliding buffer, containing 60% wt. glycerol, 10 mM HEPES (pH 7.0), 2 mM NaCl, 20 mM Ethanol, 50 μM EDTA. The reactions were run in a 3mL quartz cuvette (FP-1004, Jasco) on a Jasco FP-8300 spectrofluorometer at 20°C, continuously stirred at 800 rpm. The excitation and emission wavelengths were 520 nm and 666 nm correspondingly. The reaction read-out was FRET signal detected as a function of time. The solutions of binding partners *S* and *B* were prepared 30 minutes before the experiment in the following way. Solution 1 (binding partner *S*), final volume 2 mL, was obtained by incubating Cy5-streptavidin (43-4316, Life Technologies) with a two-fold excess

of biotin-PEG23-pVIc (custom peptide synthesis by Bio-Synthesis, Inc) in the sliding buffer to render Cy5-streptavidin molecules functionalised with pVIc. Solution 2 (binding partner *B*), final volume 1 mL, was prepared from the stock solution and contained biotin-PEG-pVIc-Cy3 in the sliding buffer. Prior to the experiments, DNA of the required length was added at a necessary concentration to both solutions. Solution 1 was transferred into the cuvette and FRET *vs.* time signal acquisition was started. Subsequently, solution 2 was rapidly injected into the cuvette with a syringe. The final reaction mix of a final volume 3 mL contained 37.5 nM Cy5-streptavidin (functionalised by 75 nM biotin-PEG23-pVIc), DNA at a chosen concentration and 150 nM binding partner *B*.

3.4.3. FRET traces analysis

The obtained FRET *vs.* time traces were initially processed using Spectra Analysis subprogram of the Spectra Manager V.2 software package by JASCO Inc. The data were subject to baseline correction, noise elimination and smoothing (binomial interpolation, 6 iterations). Subsequently, the traces were fit with a single exponential function $C(t) = C_{\max}\left[1 - \exp\left(-t/\tau\right)\right]$ and reaction times τ were extracted from the fit.

3.4.4. Single-molecule experiments

The experiments were performed in the sliding buffer (see "spectrofluorometer assay" section) using flow-stretched λ-DNA as a scaffold for sliding. Binding partner *S* was used as is; binding partner *B* was first pre-incubated with Cy5 labelled streptavidin to be able to use a 641 nm (Cy5 excitation) laser instead of a 532 nm (Cy3 excitation) one, which drastically improved the signal-to-noise ratio and allowed us to detect clearly discernible sliding along DNA. The values for binding times $\tau_{1D} \approx 0.3$ s and the 1D diffusion coefficient $D_{1D} \approx 3\times10^4$ nm^2/s (adjusted for high viscosity sliding buffer) of binding partner *S* are based on the studies of Blainey et al.[8]

3.4.5. Primer synthesis

Amino modified primers (provided by biomers.net GmbH, Table 3.2) were functionalised by the peptides in a two-step reaction.[28,29] First, lyophilised amino modified primers (1.5 mM) were reacted with a 20-fold excess of 4-(N-maleimidomethyl)cyclohexane-1-carboxylic acid 3-sulfo-N-hydroxysuccinimide ester (sulfo-SMCC) linker (Sigma Aldrich) in 0.1 M sodium phosphate buffer (pH 7.6). A stock solution of sulfo-SMCC in DMF was used. The reaction was allowed to proceed in a shaker at room temperature overnight. After incubation, the reaction mixtures were centrifuged three times using 3000 Da cut-off spin-columns (Sartorius stedim biotech) to wash out excess Sulfo-SMCC and other small molecules by Milli-Q water. The resulting solution was lyophilised and the conjugate was used for the next coupling step without further treatment. The coupling efficiency was ~50%. Lyophilised primer-SMCC conjugate was dissolved in 0.1 M sodium phosphate buffer (pH 7.6) to obtain a 200 µM solution. Subsequently, dry peptide of choice (pVIc, K or S, provided by CASLO) were added in a 5-fold molar excess. If the peptide did not dissolve completely DMF was added until a clear solution was visible. The reaction mixture was vortexed at room temperature overnight and the product was purified by reversed-phase chromatography (buffer A (pH 7.5): 0.1 M triethylammonium acetate (TEAT) containing 5% Acetonitrile; buffer B (pH 7.5): 0.1 M TEAT containing 65% Acetonitrile; column: RESOURCE RPC 1 mL; gradient: 0-60%, 50CV; wavelength: 260 nm). Finally, the buffer was exchanged to Milli-Q water by centrifugation in a 3000 Da cut-off spin-column. The products were analysed using polyacrylamide gel electrophoresis (PAGE) (Fig. 3.7) and MALDI-TOF mass spectrometry (Fig. 3.8). For further use the conjugates were lyophilised. In this reaction step, a coupling efficiency of 30 – 40% was achieved.

3.4.6. PCR reactions

Real time PCR (qPCR) experiment was performed using Bio-Rad iQ5 Real-Time PCR System (Bio-Rad Laboratories, Richmond, USA). 20 μL reaction mixtures contained forward and reverse primers (modified or unmodified) at 0.125 μM, DNA template (10 ng for circular 8669-bp M13KO7 DNA template, 5 ng for short linear 1970-bp DNA template), SYBR Green I (1×), Qiagen fast cycling PCR kit (1×) and Q-solution (1×). All reactions (unless indicated otherwise) were performed in triplicate using the following cycling protocol: initial template melting 98°C (5min); 30 cycles of [98°C (1min), 55.6°C (1s), 68°C (30s)]; 68°C (4min), 4°C (hold). The SYBR Green I fluorescence was monitored at the end of each cycle. It should be noted that the primer annealing temperature used was the one calculated for the original unmodified primers. The modified primers may have different optimal annealing temperature but, nevertheless, for all primers the same annealing temperature was used not to introduce a variable in the experiments. To compare the kinetics of amplicon formation for PCR reactions with different primers we employed the threshold cycle (C_t) analysis. The C_t was set in the exponential phase of amplification using the built-in function of the software for Bio-Rad iQ5 Real-Time PCR System. To confirm that no unspecific amplification occurs and that primer annealing step is essential in the PCR protocol we performed several control experiments (Fig. 3.9).

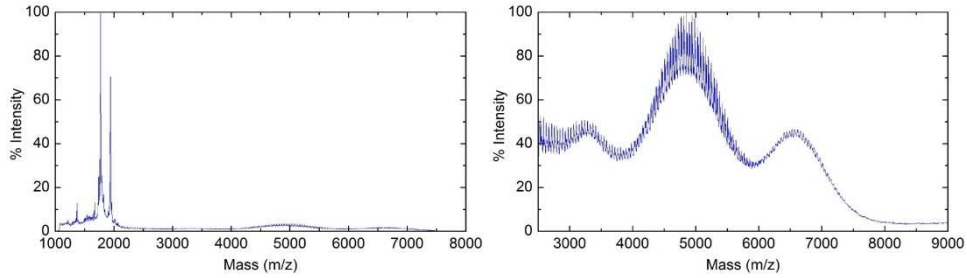

Figure 3.5 | MALDI-TOF mass spectra of binding partner *B*. Binding partner *B* is a conjugate of biotin and Cy3 labelled pVIc. Both units are connected by a poly(ethylene glycol) (PEG) linker, which exhibits a degree of polymerisation $D_P = 100$. Due to the polydisperse nature of the PEG linker a broad mass peak corresponding to binding partner *B* is obtained. The calculated molecular weight (MW) of binding partner *B* is 6700 g/mol, while the the MW determined by MALDI/TOF is 6650 g/mol. After conjugation binding partner *B* was used without further purification because unconjugated Cy3-pVIc would not bind to streptavidin and the unconjugated biotin-PEG while still possessing the ability to bind to streptavidin, would not contribute to the FRET signal.

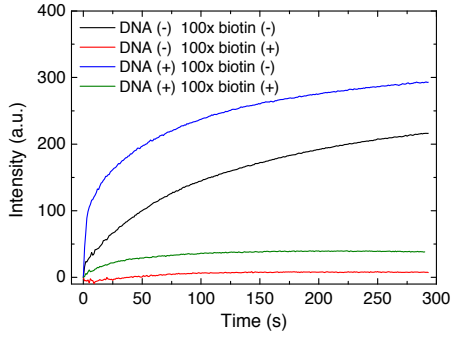

Figure 3.6 | Negative controls for the biotin-streptavidin experiment. To confirm that the rising FRET signal originates from the association between binding partners *S* and *B* we performed the control experiments for which we pre-incubated binding partner *S* with a 100x molar excess of biotin to occupy all binding pockets of streptavidin and prevent binding partner *B* from binding to them. The results for two cases are given: without DNA (black and red curves) and with 10 pM dsDNA of 2686 bp long (blue and green curves). A non-zero FRET signal in case of a 100x biotin excess might be explained by non-specific interactions between binding partners *S* and *B*.

Primer set I

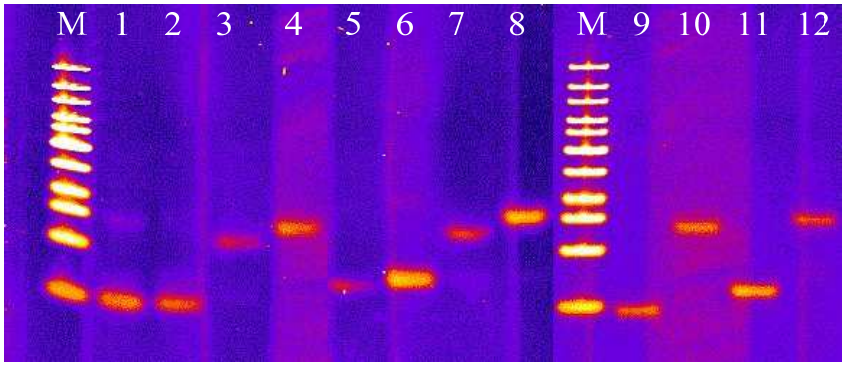

M is DNA ladder for reference (10-300 bp); Lane 1: FP;
Lane 2: FP-SMCC linker; Lane 3: FP-K; Lane 4: FP-pVIc;
Lane 5: RP; Lane 6: RP-SMCC linker; Lane 7: RP-K; Lane 8: RP-pVIc;
Lane 9: FP; Lane 10: FP-S; Lane 11: RP; Lane12: RP-S.

Primer set II

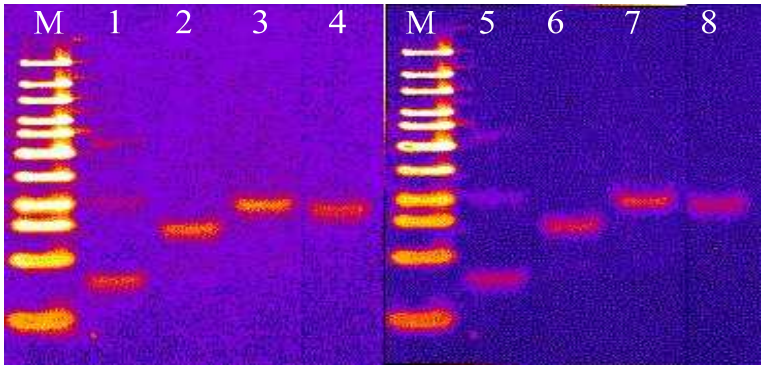

Lane 1: FP; Lane 2: FP-K; Lane 3: FP-pVIc; Lane 4: FP-S; Lane 5: RP;
Lane 6: RP-K; Lane 7: RP-pVIc; Lane 8: RP-S.

Figure 3.7 | Analysis of primer-peptide conjugates by polyacrylamide gel electrophoresis (PAGE) after chromatographic purification. The purity of forward (FP) and reverse (RP) primer-peptide conjugates was analysed using a 20% PAGE gel with subsequent SYBR Gold staining.

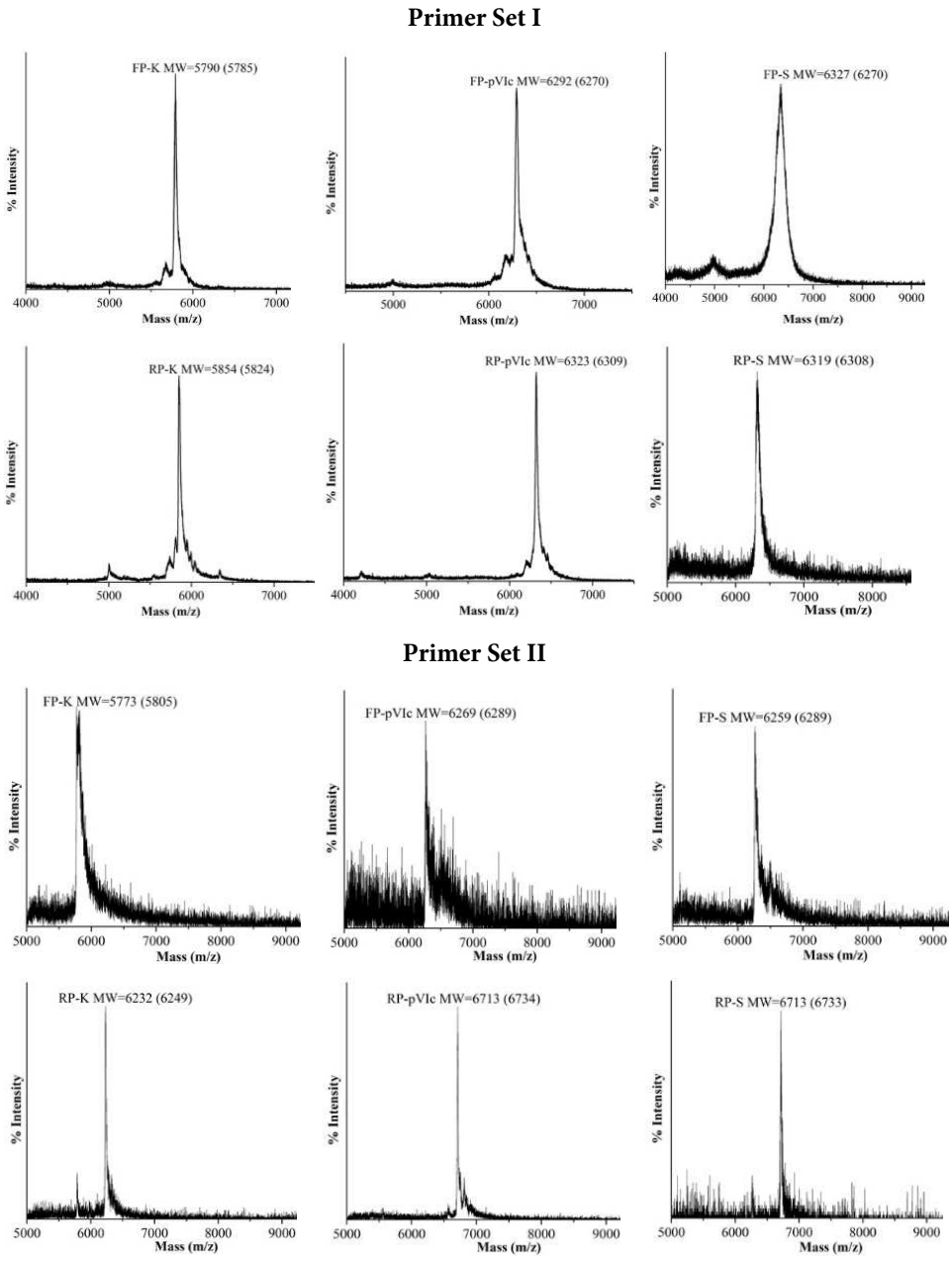

Figure 3.8 | MALDI-TOF mass spectra of primer-peptide conjugates. The molecular weights (MW) obtained from the measurements are shown above the peaks. The predicted MW are given in brackets.

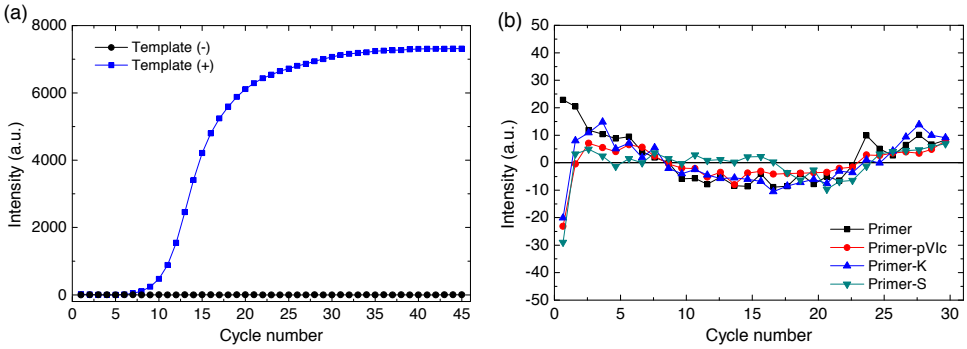

Figure 3.9 | qPCR control experiments. (a) Unmodified primers were used in qPCR with and without DNA template to detect if any unspecific DNA amplification occurred. A 20 µL reaction mixture contained pristine forward and backward primer (primer set I) at a concentration of 0.5 µM, 10 ng DNA template (circular dsDNA of 8669 bp length that originated from bacteriophage M13KO7), Sybr Green I (1×), Qiagen fast cycling PCR kit (1×) and Q-solution (1×). The following qPCR protocol was used: 98°C (5min); 45 cycles of [98°C (1min), 55.6°C (15s), 68°C (30s)]; 68°C (4min), 4°C (hold). When the template was omitted, no amplicon generation was detected indicating that unspecific DNA amplification does not occur. (b) To confirm that PCR product formation depends on primer hybridisation on the template and that the annealing of modified and unmodified primers does not occur during the elongation step we performed the qPCR experiment without the annealing step during thermal cycling. The PCR conditions were selected as described above for panel (a) except for an altered thermal cycling protocol: 98°C (5min); 30 cycles of [98°C (1min), 68°C (30s)]; 68°C (4min), 4°C (hold). No amplicon formation is detected for any of the primers indicating that the annealing step within the thermal cycling protocol is critical for product formation.

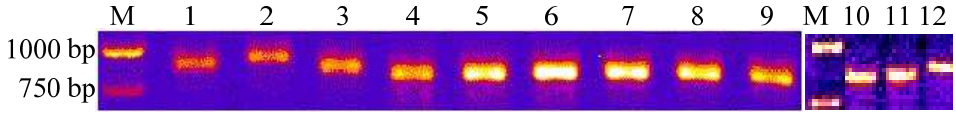

Lane M: DNA ladder; Lane 1-3: amplicon from unmodified primers; Lane 4-6: amplicon from primer-K; Lane 7-9: amplicon from primer-pVIc; Lane 10-12: amplicon from primer-S.

Figure 3.10 | Amplicon formation. The formation of the amplicon of the correct length was confirmed using a 2% agarose gel.

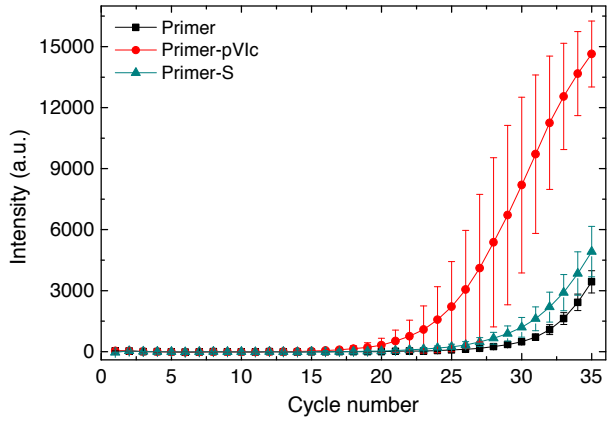

Figure 3.11 | qPCR using primer set II. To prove the general applicability of the sliding peptides to speed up PCR we conducted the qPCR experiments with a different set of primers (Primer set II, Table 3.2). For qPCR conditions and the template see legend to Fig. 3.9. Error bars represent standard deviation based on experiments in triplicate.

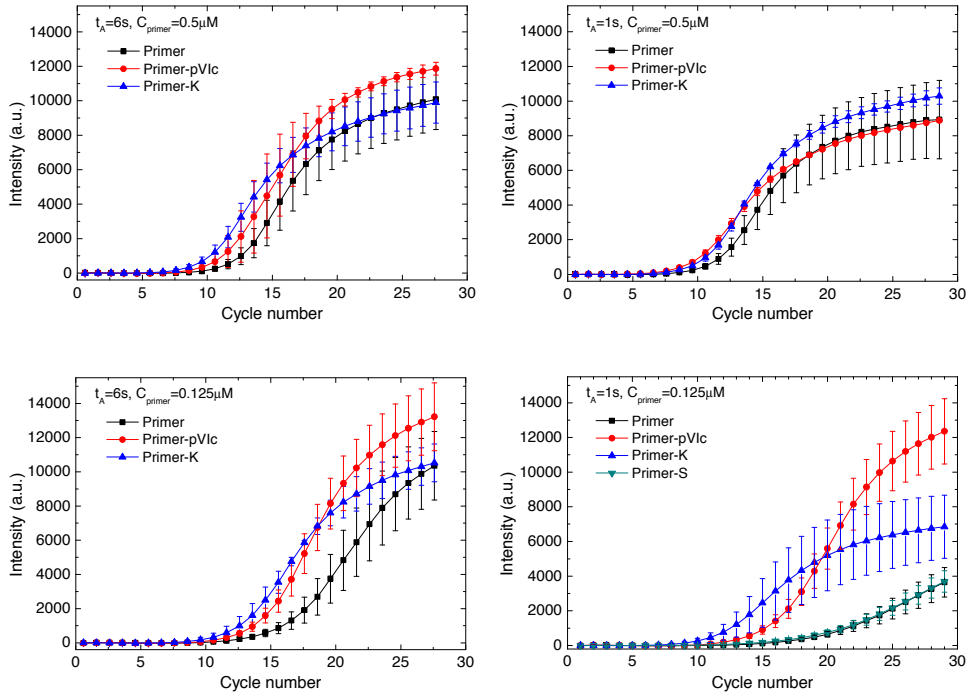

Figure 3.12 | Performance comparison of different primer-peptide modifications under different PCR conditions. The qPCR reactions for primer set I, template 8669 bp dsDNA M13KO7 were performed using different annealing times and primer concentrations. The annealing times in qPCR protocol (for protocol see legend to Fig. 3.9) were 1 s and 6 s and two primer concentrations were 0.5 µM and 0.125 µM. Low primer concentrations and low annealing times (the most stringent conditions) gave the highest speed-up of PCR amplification compared to higher annealing times and primer concentration. Error bars represent standard deviation based on experiments in triplicate.

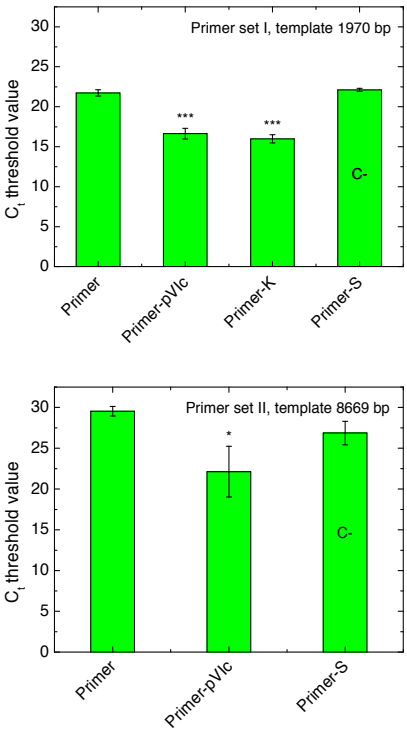

Figure 3.13 | Performance comparison of different primer-peptide conjugates in their ability to speed up the PCR. Two different pairs of primers and templates were used. Cycle threshold values C_t were extracted from qPCR traces. Statistical test for significance was unpaired t-test with unequal variance. ***p<0.001, **p<0.01, *p<0.05. Error bars indicate ±SD; n = 3.

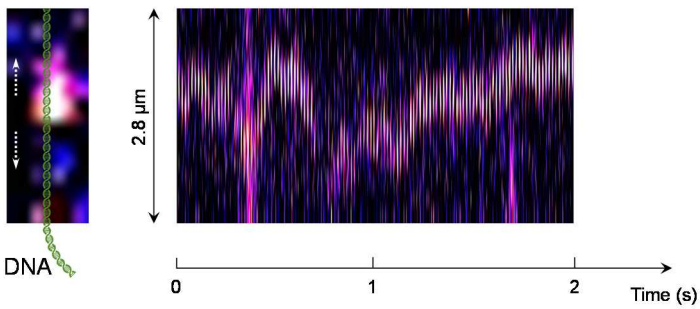

Figure 3.14 | Single-molecule experiments on the sliding of K-peptide. To confirm that peptide K (truncated pVIc) retained the ability to slide, single-molecule experiments were performed on this peptide carrying a fluorophore at the cysteine. The average diffusion coefficient $D_{K-peptide} = 22.12 \times 10^6$ bp²/s, which corresponds to the values measured for pVIc.

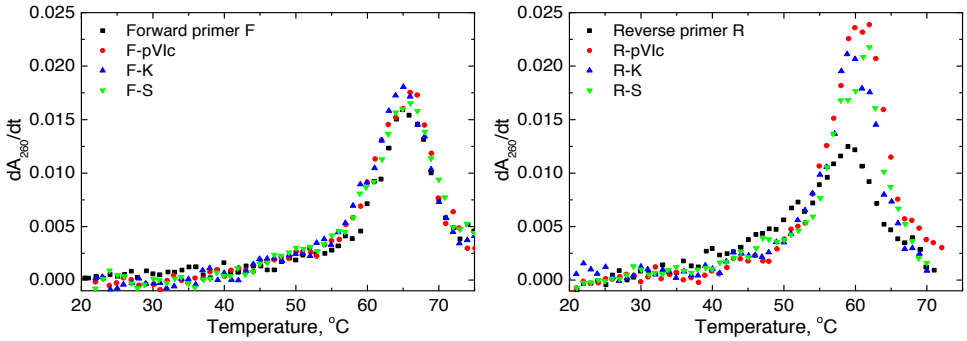

Figure 3.15 | Primer melting temperature measurements. The melting temperatures T_m of the modified and unmodified primers from the primer set II (see Table 3.2) were measured. The absorption at 260 nm was detected while increasing the temperature with a rate of 0.5°C/min starting from 20°C. The measurements were performed using primer-complementary oligo's; the hybridisation buffer was: 10 mM $MgCl_2$, 50 mM NaCl and 10 mM Tris, pH=7.5. The experiments were done in duplicate; the figure shows one set of experiments, the results are depicted as the first derivative of the absorption (260 nm). The obtained T_m values are:

Primer	T_m, °C
F	65.5 ± 0.5
F-pVIc	65.5 ± 0.5
F-K	65
F-S	65 ± 1
R	59.5 ± 0.5
R-pVIc	62
R-K	60 ± 1
R-S	61.5 ± 0.5

Table 3.1. Double stranded DNA sequences used in the proof-of-principle reaction studies.

DNA length	DNA sequence
15 bp	5'-GCC TCG CCG CGC CCC-3' (Custom DNA synthesis by Integrated DNA technologies)
50 bp	5'-AGA CAG CAT CGG AAC GAG GGT AGC AAC GGC AAC AGA GGC TTT GAG GAC TA-3' (Custom DNA synthesis by Integrated DNA technologies)
100 bp	5'-ATG CGC CTG GTC TGT ACA CCG TTC ATC TGT CCT CTT TCA AAG TTG GTC AGT TCG GTT CCC TTA TGA TTG ACC GTC TGC GCC TCG TTC CGG CTA AGT AAC A-3' (Custom DNA synthesis by Integrated DNA technologies)
150 bp	5'-TTG AAA AAG CCG TTT CTG TAA TGA AGG AGA AAA CTC ACC GAG GCA GTT CCA TAG GAT GGC AAG ATC CTG GTA TCG GTC TGC GAT TCC GAC TCG TCC AAC ATC AAT ACA ACC TAT TAA TTT CCC CTC GTC AAA AAT AAG GTT ATC AAG TGA-3' (Initially amplified from a kanamycin resistance gene (F primer: 5'-TTG AAA AAG CCG TTT CTG TAA TGA AGG AGA AAA CTC-3', R-primer: 5'-TCA CTT GAT AAC CTT ATT TTT GAC GAG GGG AAA TTA-3') Subsequently amplified using 150mer itself as a template. Purified by ethanol precipitation)
300 bp	5'-AGT GCG ATT AAG CCA GAC ATG AAG ATC AAA CTC CGT ATG GAA GGC AAC GTA AAC GGG CAC CAC TTT GTG ATC GAC GGA GAT GGT ACA GGC AAG CCT TTT GAG GGA AAA CAG AGT ATG GAT CTT GAA GTC AAA GAG GGC GGA CCT CTG CCT TTT GCC TTT GAT ATC CTG ACC ACT GCA TTC CAT TAC GGC AAC AGG GTA TTC GCC AAA TAT CCA GAC AAC ATA CAA GAC TAT TTT AAG CAG TCG TTT CCT AAG GGG TAT TCG TGG GAA CGA AGC TTG ACT TTC GAA GAC GGG GGC ATT TGC-3' (Initially amplified from pNZ-mEos3.2 plasmid (F primer: 5'- AGT GCG ATT AAG CCA GAC ATG AAG ATC AAA CTC CGT-3', R primer: 5'- GCA AAT GCC CCC GTC TTC GAA AGT CAA GCT TCG T-3') Subsequently amplified using 300mer itself as a template. Purified by ethanol precipitation)

934 bp	5'-CGC GAG CAT AAT AAA CGG CTC TGA TTA AAT TCT GAA GTT TGT TAG ATA CAA TGA TTT CGT TCG AAG GAA CTA CAA AAT AAA TTA TAA GGA GGC ACT CAC CAT GGG AAG TGC GAT TAA GCC AGA CAT GAA GAT CAA ACT CCG TAT GGA AGG CAA CGT AAA CGG GCA CCA CTT TGT GAT CGA CGG AGA TGG TAC AGG CAA GCC TTT GAG GGA AAA CAG AGT ATG GAT CTT GAA GTC AAA GAG GGC GGA CCT CTG CCT TTT GCC TTT GAT ATC CTG ACC ACT GCA TTC CAT TAC GGC AAC AGG GTA TTC GCC AAA TAT CCA GAC AAC ATA CAA GAC TAT TTT AAG CAG TCG TTT CCT AAG GGG TAT TCG TGG GAA CGA AGC TTG ACT TTC GAA GAC GGG GGC ATT TGC AAC GCC AGA AAC GAC ATA ACA ATG GAA GGG GAC ACT TTC TAT AAT AAA GTT CGA TTT TAT GGT ACC AAC TTT CCC GCC AAT GGT CCA GTT ATG CAG AAG AAG ACG CTG AAA TGG GAG CCC TCC ACT GAG AAA ATG TAT GTG CGT GAT GGA GTG CTG ACG GGT GAT ATT GAG ATG GCT TTG TTG CTT GAA GGA AAT GCC CAT TAC CGA TGT GAC TTC AGA ACT ACT TAC AAA GCT AAG GAG AAG GGT GTC AAG TTA CCA GGC GCC CAC TTT GTG GAC CAC TGC ATT GAG ATT TTA AGC CAT GAC AAA GAT TAC AAC AAG GTT AAG CTG TAT GAG CAT GCT GTT GCT CAT TCT GGA TTG CCT GAC AAT GCC AGA CGA TAA CTG CAG GCA TGC GGT ACC ACT AGT TCT AGA GAG CTC AAG CTT TCT TTG AAC CAA AAT TAG AAA ACC AAG GCT TGA AAC GTT CAA TTG AAA TGG CAA TTA AAC AAA TTA CAG CAC GTG TTG CTT TGA TTG ATA GCC AAA AAG CAG CAG TTG-3' (Initially amplified from pNZ-mEos3.2 plasmid (F primer: 5'-CGC GAG CAT AAT AAA CGG CTC TG-3', R primer: 5'-CAA CTG CTG CTT TTT GGC TAT C-3') Subsequently amplified using 934mer itself as a template. Purified by ethanol precipitation)
2686 bp	pUC19 vector (N3041L, New England Biolabs)

Table 3.2. Primer sets used in PCR experiments.

Primer set I	Forward: 5'-(NH_2)-CTC ATC GAG CAT CAA-3' Reverse: 5'-(NH_2)-ATG AGC CAT ATT CAA-3'	807 bp amplicon
Primer set II	Forward: 5'-(NH_2)-GCG TTT CCT CGG TTT-3' Reverse: 5'-(NH_2)-GTA ATT TAG GCA GAG G-3'	831 bp amplicon

3.5. References

1. M. Dlugosz and J. Trylska, *BMC Biophys.*, 2011, **4**, 1-9.
2. A. D. Riggs, S. Bourgeois and M. Cohn, *J. Mol. Biol.*, 1970, **53**, 401-417.
3. S. Chatterjee and E. Rothenberg, *Viruses*, 2012, **4**, 3162-3178.
4. S. Redding and E. C. Greene, *Chem. Phys. Lett.*, 2013, **570**, 1-11.
5. O. G. Berg, R. B. Winter and P. H. von Hippel, *Biochem.*, 1981, **20**, 6929-6948.
6. A. Tafvizi, L. A. Mirny and A.M. van Oijen, *ChemPhysChem*, 2011, **12**, 1481-1489.
7. V. Graziano, G. Luo, P. C. Blainey, A. J. Péres-Berná, W. J. McGrath, S. Jane Flint, C. San Martín, X. Sunney Xie and W. F. Mangel, *The J. of Biol. Chem.*, 2013, **288**, 2068-2080.
8. P. C. Blainey, V. Graziano, A. J. Péres-Berná, W. J. McGrath, S. Jane Flint, C. San Martín, X. Sunney Xie and W. F. Mangel, *The J. of Biol. Chem.*, 2013, **288**, 2092-2102.
9. A. J. Pérez-Berná, R. Marabini, S. H. W. Scheres, R. Menéndez-Conejero, I. P. Dmitriev, D. T. Curiel, W. F. Mangel, S. J. Flint and C. San Martín, *J. Mol. Biol.*, 2009, **392**, 547-557.
10. W. F. Mangel, M. L. Baniecki and W. J. McGrath, *Cell. Mol. Life Sci.*, 2003, **60**, 2347-2355.
11. W. F. Mangel, W. J. McGrath, D. L. Toledo and C. W. Anderson, *Nature*, 1993, **361**, 274-275.
12. T. W. J. Gadella, *FRET and FLIM Techniques*, Elsevier Science, Oxford, UK, 2009.
13. J. P. Peters, N. A. Becker, E. M. Rueter, Z. Bajzer, J. D. Kahn and L. J. Maher, *Methods Enzymol.*, 2011, **488**, 287-335.
14. Q. Du, C. Smith, N. Shiffeldrim, M. Vologodskaia and A. Vologodskii, *Proc. Nat. Acad. Sci. U. S. A.*, 2005, **102**, 5397-5402.
15. C. G. Baumann, S. B. Smith, V. A. Bloomfield and C. Bustamante, *Proc. Nat. Acad. Sci. U. S. A.*, 1997, **94**, 6185-6190.
16. A. Turkin, A. M. van Oijen and A. A. Turkin, *Phys. Rev. E: Stat., Nonlinear, Soft Matter Phys.,* 2015, DOI: 10.1103/PhysRevE.92.052703.
17. S. Kennedy and N. Oswald, *PCR Troubleshooting and Optimization: The Essential Guide*, Caister Academic Press, Norfolk, UK, 2011.
18. J. Wilhelm and A. Pingoud, *ChemBioChem*, 2003, **4**, 1120-1128.
19. I. V. Kutyavin, I. A. Afonina, A. Mills, V. V. Gorn, E. A. Lukhtanov, E. S. Belousov, M. J. Singer, D. K. Walburger, S. G. Lokhov, A. A. Gall, R. Dempcy, M. W. Reed, R. B. Meyer and J. Hedgpeth, *Nucleic Acids Res.*, 2000, **28**, 655-661.
20. I. Afonina, M. Zivarts, I. Kutyavin, E. Lukhtanov, H. Gamper and R. B. Meyer, *Nucleic Acids Res.*, 1997, **25**, 2657–2660.
21. B. Frey and B. Suppmann, *Biochemica*, 1995, **2**, 34-35.

22. Y. Wang, D. E. Prosen, L. Mei, J. C. Sullivan, M. Finney and P. B. Vander Horn, *Nucleic Acids Res.*, 2004; **32**, 1197-1207.
23. J. F. Davidson, R. Fox, D. D. Harris, S. Lyons-Abbott and L. A. Loeb, *Nucleic Acids Res.*, 2003, **31**, 4702-4709.
24. M. Motz, I. Kober, C. Girardot, E. Loeser, U. Bauer, M. Albers, G. Moeckel, E. Minch, H. Voss, C. Kilger, and M. Koegl, *J. Biol. Chem.*, 2002, **277**, 16179-16188.
25. M. W. Kanan, M. M. Rozenman, K. Sakurai, T. M. Snyder and D. R. Liu, *Nature*, 2004, **431**, 545–549.
26. M. L. McKee, P. J. Milnes, J. Bath, E. Stulz, A. J. Turberfield and R. K. O'Reilly, *Angew. Chem. Int. Ed.*, 2010, **49**, 7948-7951.
27. Y. Li, P. Zhao, M. Zhang, X. Zhao and X. Li, *J. Am. Chem. Soc.*, 2013, **135**, 17727-17730.
28. C.H. Tung, M.J. Rudolph, S. Stein, *Bioconj. Chem.*, 1991, **2**, 464-465.
29. A.W. Fraley, B. Pons, D. Dalkara, G. Nullans, J.-P. Behr and G. Zuber, *J. Am. Chem. Soc.*, 2006, **128**, 10763-10771.